**Atmospheric
Chemistry
and Physics
Discussions**

**ACPD**

8, 12197–12225, 2008

Synoptic CO$_2$
mechanisms

N. Parazoo et al.

Title Page

Abstract | Introduction

Conclusions | References

Tables | Figures

◄◄ | ►►

◄ | ►

Back | Close

Full Screen / Esc

Printer-friendly Version

Interactive Discussion

# Mechanisms for synoptic transport of atmospheric CO$_2$ in the midlatitudes and tropics

N. Parazoo[1], A. Denning[1], S. Kawa[2], K. Corbin[1], R. Lokupitiya[1], and I. Baker[1]

[1]Atmospheric Science Department, Colorado State University, Fort Collins, Colorado, USA
[2]NASA Goddard Space Flight Center, Greenbelt, Maryland, USA

Correspondence to: N. Parazoo (nparazoo@atmos.colostate.edu)

## Abstract

Synoptic variations of $CO_2$ mixing ratio produced by interactions between weather and surface fluxes are investigated mechanistically and quantitatively in midlatitude and tropical regions using continuous in-situ $CO_2$ observations in North America, South America and Europe and forward chemical transport model simulations with the Parameterized Chemistry Transport Model. Frontal $CO_2$ climatologies show consistently strong, characteristic frontal $CO_2$ signals throughout the midlatitudes of North America and Europe. Transitions between synoptically identifiable $CO_2$ air masses or transient spikes along the frontal boundary typically characterize these signals. One case study of a summer cold front shows that $CO_2$ gradients organize with deformational flow along weather fronts producing strong and spatially coherent variations. A boundary layer budget equation is constructed in order to determine contributions to boundary layer $CO_2$ tendencies by horizontal and vertical advection, moist convection, and biological and anthropogenic surface fluxes. Analysis of this equation suggests that, in midlatitudes, advection is responsible for 50–90% of the amplitude of frontal variations in the summer, depending on upstream influences, and 50% of all day-to-day variations throughout the year. Simulations testing sensitivity to local cloud and surface fluxes further suggest that horizontal advection is a major source of $CO_2$ variability in midlatitudes. In the tropics, coupling between convective transport and surface $CO_2$ flux is most important. Due to the scarcity of tropical observations available at the time of this study, future work should extend such mechanistic analysis to additional tropical locations.

## 1 Introduction

Continuous in-situ measurements of atmospheric $CO_2$ over midlatitude and tropical regions exhibit synoptic variations strongly influenced by coupling between weather and surface $CO_2$ flux (e.g. Law et al., 2002; Gerbig et al., 2003; Geels et al., 2004; Lin

et al., 2004). Weather differences in the midlatitudes and tropics can be explained in part by the different energy reserves available in the atmosphere. In the tropics, latent heat release associated with cumulus convection is the significant source of energy for weather (Holton, 1992). Although latent heat is important in midlatitudes, it is generally thought to be a secondary energy source for synoptic weather. Midlatitude synoptic scale weather disturbances derive energy from the zonal available potential energy associated with latitudinal temperature gradients (baroclinicity). In the tropics, because of weak temperature gradients and negligible Coriolis, baroclinic effects are weak. Due to energy constraints, horizontal mixing is more prevalent in midlatitudes while vertical convective mixing is more prevalent in the tropics.

Figure 1 shows midday planetary boundary layer (PBL) $CO_2$ (given as a mole fraction in units of parts per million (ppm)), from sites in North America, South America and Europe, where midday maximizes the amount regional and synoptic influence compared to local influence during well-mixed boundary layer conditions (Bakwin et al., 1998). Synoptic variations of 10–20 ppm over 1–3 days are common, comparable to seasonal amplitudes. Continental variations under terrestrial influence are typically much stronger than in remote mountainous and maritime locations. A comparison of monthly standard deviation of midday values at continental (e.g. LEF, HRV, and HEI) and remote (e.g. MLO, BRW, and ZEP) sites verifies this (Fig. 1).

Davis et al. (2003) observed that daily PBL $CO_2$ tendencies at a site in Northern Wisconsin are governed primarily by local net ecosystem exchange (NEE, defined as gross primary production minus ground respiration) during fair weather. During May and September, however, the sign of NEE was contradictory to $CO_2$ tendencies expected from NEE of $CO_2$. Preliminary investigation explained this through the presence of discrete non-fair weather events such as frontal passage. Whether the source for such variations was horizontal or vertical advection could not be explained.

In non-fair weather events, such as surface cold fronts, mechanisms for synoptic variations that have been proposed in the literature include: 1) nonlocal influence through lateral advection of upstream horizontal $CO_2$ gradients, 2) vertical motion through moist

convection and frontal lifting over air mass boundaries along frontal zones, and 3) ecosystem respiration and photosynthesis response to frontal weather. Several studies (e.g. Worthy et al., 2003; Chan et al., 2004; Geels et al., 2004; Corbin and Denning, 2006) have investigated the role of horizontal advection. These studies conclude that horizontal advection of remotely generated $CO_2$ anomalies is an important source for downstream variations. Chan et al. (2004) also found that biospheric fluxes are strongly coupled to radiative forcing changes under cloud cover associated with fronts.

This study investigates and quantifies mechanisms responsible for synoptic variations in midlatitudes and the tropics using well-calibrated continuous observations from 17 sites across the globe, global transport model simulations, and boundary layer budget analysis. The remainder of the paper is organized as follows: Sect. 2 describes the simulation models and $CO_2$ observations, Sect. 3 discusses the observed and simulated midlatitude and tropical synoptic variations, and Sect. 4 summarizes results.

## 2 Methods

### 2.1 Observations

Continuous $CO_2$ observations are utilized in this study to investigate variations continuously in time at a point in space. These data were collected from well-calibrated continuous stations in North America, South America, and Europe. Midday values (the mixing ratio averaged from 1–5 pm local time) were used from hourly time series to investigate day-to-day variability. Although the range of measurement heights varies from 9–457 m a.g.l., only measurements between 9–40 m were included in the analysis for consistency. The use of midday values ensures that the boundary layer is well mixed such that $CO_2$ values near the surface and those near the top of the PBL have similar mixing ratios. This also helps to maximize comparison to transport simulations, which struggle to capture concentrations during stable periods. Figure 2 shows the location of each site. Table 1 gives a brief description of each site. Descriptions

Full Screen / Esc

Printer-friendly Version

Interactive Discussion

of the majority of these sites can also be found at http://www.esrl.noaa.gov/gmd/ and http://gaw.kishou.go.jp/wdcgg/.

## 2.2 Models and driver data

The Parameterized Chemistry Transport Model (PCTM) was used for forward global simulations of $CO_2$ transport (e.g. Kawa et al., 2004). This provides a diagnostic tool for studying synoptic interactions among weather and surface $CO_2$ flux. Transport fields were provided by NASA's Goddard Earth Observation System, version 4 (GEOS4), data assimilation system (GEOS4-DAS) (Bloom et al., 2005) and include 6-hourly analyzed winds, temperatures, diffusion coefficients, and convective mass fluxes. Physical parameterizations are derived from the National Center for Atmospheric Research Community Climate Model, Version 3 (Kiehl et al., 1998). Subgrid scale vertical processes include cumulus convection (cloud mass flux (CMF) from deep (Zhang and McFarlane, 1995) and shallow (Hack et al., 1994) parameterized convection) and turbulence parameters. Surface $CO_2$ fluxes include hourly NEE from the Simple Biosphere Model, Version 3 (SiB3), constant in time anthropogenic fossil fuel emissions (FF) (Andres et al., 1996), and monthly air-sea exchange (OCEAN) of $CO_2$ (Takahashi et al., 2002). Fire emissions are ignored.

SiB is a land-surface parameterization scheme originally used to simulate biophysical processes in climate models (Sellers et al., 1986), but later adapted to include ecosystem metabolism (Sellers et al., 1996a; Denning et al., 1996). SiB involves the direct calculation of carbon assimilation by photosynthesis to calculate land-atmosphere $CO_2$ exchange (Denning et al., 1996; Sellers et al., 1996a). The soil representation is similar to that of CLM (Dai et al., 2003), with 10 soil layers and an initial soil column depth of 3.5 m. SiB has been updated to include prognostic calculation of temperature, moisture, and trace gases in the canopy air space, and the model has been evaluated against eddy covariance measurements at a number of sites (Baker et al., 2003; Hanan et al., 2005; Vidale and Stockli, 2005). We refer to this base version of the code as SiB3.

**Synoptic $CO_2$ mechanisms**

N. Parazoo et al.

SiB3 was run in steady state mode in which ecosystem respiration balances gross primary production over one year at every grid point. The meridional gradient and secular trends simulated by the model are therefore stronger than observed (Kawa et al., 2004), but we focus on synoptic time scales. Flux and energy calculations in SiB3 were driven by GEOS4-DAS meteorology. GEOS4 precipitation was scaled by monthly precipitation from the Global Precipitation Climatology Project (GPCP) (Huffman et al., 2001) to force total monthly precipitation in GEOS4 to match that of GPCP. The time at which precipitation occurs remained unchanged so that covariance of anomalies in cloudiness, moisture, and vertical transport is conserved.

Details of PCTM and the experimental setup are similar to Kawa et al. (2004). PCTM was run from 2000–2004 at 1.25° by 1° (longitude by latitude) with 25 levels to 1 mbar, where 2000–2002 comprised the spin up period to establish the interhemispheric $CO_2$ gradient.

## 3 Discussion

### 3.1 Frontal $CO_2$

As discussed in Sect. 1, discrete frontal passage events in the spring and autumn can cause $CO_2$ mixing ratios that are inconsistent with the sign of local NEE. Frontal systems, however, occur all year in midlatitudes, and may therefore be responsible for causing variations regardless of local surface fluxes. We can start thinking about the role of cold fronts in redistributing $CO_2$ throughout the atmosphere by briefly discussing cold front dynamics. Fronts are a result of baroclinicity, in which differential solar heating between the equator and pole brings about meridional temperature gradients that tend to concentrate in baroclinic zones associated with tropospheric jet streams. Through instabilities, baroclinic waves can then remove available potential energy from the mean flow and provide energy for the development of synoptic scale storms, such as cold fronts, which act to reduce horizontal temperature gradients by mixing thermo-

dynamically unique air masses; i.e. transporting relative cold dry air south and warm moist air north.

By analyzing $CO_2$ mixing ratio signals during frontal passage over multiple frontal events and averaging the signals together, we find that cold fronts are indeed important for producing strong downstream variations and, furthermore, that these variations are persistent throughout the year. Figure 3 shows climatologies of simulated and observed growing season (June–September) frontal $CO_2$ events at continuous sites in North America and Europe. Winter climatologies (December–February) are shown in Fig. 4.

The procedure for creating these climatologies is as follows. First, some general way of defining frontal zones in which frontal signals occur is needed. This study focuses on surface-based cold fronts in part because their surface signatures tend to be more sharply defined than other surface fronts, making them easier to identify and study (Schultz, 2005). We characterize surface fronts according to the Clarke and Renard (1965) definition, who define a front as "the warm-air boundary of a synoptic-scale baroclinic zone of distinct thermal gradient... Further, the frontal-zone boundaries are considered as quasi first-order thermal and moisture discontinuities." Temporal gradients of temperature and water vapor are used together with clockwise wind shifts and pressure minima to locate the warm-air boundary. Other frontal weather fields such as precipitation and radiation were not used to classify fronts. Although important for NEE (Chan et al., 2004) such classification was beyond the scope of this study.

Surface pressure and 10 m wind, temperature, and specific humidity from GEOS4-DAS were used to identify the time of frontal passage at all of the continuous $CO_2$ sites. The long-term trend and diurnal/seasonal cycles were removed from the temperature and specific humidity time series using a butterworth filter until only synoptic variations remained, which we define to occur at a frequency range of 1–10 days. Frontal passage was then approximated as the time at which the second order gradients in specific humidity and temperature were at their maxima over the synoptic time scale (1–5 days), concurrent with a clockwise wind shift and approximate pressure minima. Since only

Printer-friendly Version

Interactive Discussion

3-hourly reanalysis was available for this analysis, all times are approximate. Figure 5, which shows the summer climatology (averaging procedure discussed below) of the observed and simulated meteorology at three sites in North America, demonstrates that the timing of fronts identified in the reanalysis are consistent with observations.

After identifying particular events, the long-term trend and diurnal/seasonal cycles were removed from observed hourly and simulated 3-hourly $CO_2$ time series. Frontal composites were constructed by averaging synoptic anomalies at each station from 48 h before frontal passage until 48 h after. The result is the average frontal signal that the station observes (and simulates) as the front passes by. The signals in Figs. 3 and 4 vary with time at a point in space defined by the station, where time increases on the x-axis from left to right with zero representing the time of frontal passage and negative (positive) time anomalies representing the signal before (after) frontal passage.

Focusing for now on the growing season, frontal climatologies suggest that some sites (e.g. SGP, WKT, SBI, and WPL) feature air mass replacement of higher prefrontal $CO_2$ with lower postfrontal $CO_2$. At other sites $CO_2$ variations occur as transient spikes during frontal passage (e.g. CDL, AMT, and ZEP). The top and middle plots of Fig. 6, which show July mean NEE and FF over North America, combined with the frontal identification constraint discussed earlier that all frontal events used in the frontal climatologies exhibit clockwise wind shifts characteristic of cold fronts in which the wind is generally from the south prior to frontal passage and from the north afterwards, helps to explain the nature of these signals and why they vary between sites. When maps of NEE, FF, and OCEAN are combined into the time mean (bottom plot of Fig. 6) we find a quite diverse pattern of influence unique to each site (site location plotted for convenience).

SGP and WKT, for example, exhibit a frontal signal in which $CO_2$ mixing ratios decrease over the course of frontal passage. According to Fig. 6, the region containing these sites is dominated by positive surface flux while the region to the north is dominated by negative surface flux. This creates a north-south gradient in surface flux which, when under the influence of fair weather typical of a high-pressure system, is

expected to create relatively $CO_2$ depleted air masses to the north and $CO_2$ enriched air masses to the south. If air is then advected from the north as a low-pressure system settles in and frontal passage ensues, as might be expected due to typical wind patterns associated with fronts, this would help to explain the decreasing $CO_2$ tendency associated with frontal signals observed at SGP and WKT. Such unique upstream surface flux influences (each site is different), combined with horizontal advection along cold fronts (see Sect. 3.2), help to interpret these frontal $CO_2$ signals.

## 3.2 Budget analysis

Since PCTM reproduces much of the amplitude, shape, and phase of the observed composite surface signals in Figs. 3 and 4, we turn to an analysis of model output to study physical and biological mechanisms active along fronts to determine the role of advection in the frontal $CO_2$ signatures discussed above. Diagnosis of simulated advective tendencies associated with frontal climatologies illustrates the importance of advection compared to surface flux and moist convection during frontal passage.

$$\underbrace{\frac{\partial C}{\partial t}}_{i} + \underbrace{\frac{RT}{p}\frac{F_c}{z_1}}_{ii} + \underbrace{K_m\frac{\partial C}{\partial z}}_{iii} + \underbrace{W\frac{\partial C}{\partial z}}_{iv} + V_H \cdot \nabla_H C_v + \underbrace{g\frac{M\partial C}{\partial p}}_{vi} = 0 \qquad (1)$$

Equation (1) represents the simulated $CO_2$ tendency (i) due to surface flux (ii), vertical diffusion (iii), vertical advection (iv), horizontal advection (v), and vertical cloud transport, where $C$ is $CO_2$ mixing ratio in ppm, $F_c$ is the surface flux due to NEE, FF, and OCEAN, $z_1$ is the lowest model level ($\sim$50 m), $R$ is the gas constant, $T$ is temperature, $p$ is pressure, $K_m$ is the vertical diffusion coefficient, $W$ is vertical velocity, $V_H$ is the horizontal wind, $g$ is gravity, and $M$ is net convective mass flux as described in the work of Kawa et al. (2004).

To gauge relative importance, each term was output from PCTM every hour (terms (ii) and (iii) together represent vertical diffusion of surface flux). Hourly tendencies at each layer within the PBL were averaged through the three lowest model levels and

|◀ | ▶|

◀ | ▶

Back | Close

Full Screen / Esc

Printer-friendly Version

Interactive Discussion

then converted to daily averaged tendencies, where level three (approximately 500 m above the surface) is assumed to represent the PBL height at all times such that the dominance of shallow nocturnal PBL's on surface flux tendencies is reduced. The resulting terms represent synoptic PBL CO$_2$ tendencies. The sum of the advective tendencies were divided by the sum of all tendencies, and then averaged across the same events used in the frontal climatologies, to represent the fractional contribution of advection to frontal CO$_2$ variations (dashed lines in Figs. 3 and 4).

An example of annual mean percent contributions at several sites in North and South America are shown in Table 2. These values are discussed in Sect. 3.3. For now discussion is limited to frontal events. This method suggests that daily average advective contribution is approximately 60% during frontal passage in the summer, ranging from about 30% where local surface flux (NEE+FF) tendencies dominate (e.g. FRS and PAL) to above 75% where advection dominates (islands like MHD, ZEP and SBI and remote regions like BRW and ALT). Vertical cloud transport accounts for about 8% of frontal CO$_2$ tendencies on average. Advection accounts for a larger percentage in the winter (69%) when NEE is weaker.

### 3.3 Deformational flow

Transient variations associated with frontal passages are interpreted in a case study of a simulated low-pressure system near FRS. Figure 7 shows daily snapshots of surface CO$_2$ and wind vectors in the days leading up to a spike at FRS. In this example, several positive CO$_2$ anomalies (SW quadrant of 7a and 7b) have formed ahead of the developing cyclone (NW quadrant of 7b) due, in this case, to persistent positive NEE and advection of FF generated anomalies from the east (not shown). The anomalies merge together in the wind shear south of the cyclone. On day 3 (7c) the anomalies become aligned with the front and advect to the east during day 4 (7d). The preexisting NE-SW CO$_2$ gradient was organized and concentrated into a narrow frontal zone of high CO$_2$ by deformational flow.

Deformational flow is the basis for the theory presented in this paper to explain the or-

ganization of $CO_2$ along cold fronts, which, through converging and shearing wind fields along frontal boundaries, acts to stretch and shear tracers in the flow. Holton (1992) used kinematic theory and an equation similar to Eq. (2):

$$\frac{D_g}{Dt}\left(\frac{\partial C}{\partial x} + \frac{\partial C}{\partial y}\right) = -\underbrace{\frac{\partial u_g}{\partial x}\frac{\partial C}{\partial x}}_{\text{I}} - \underbrace{\frac{\partial v_g}{\partial x}\frac{\partial C}{\partial y}}_{\text{II}} - \underbrace{\frac{\partial u_g}{\partial y}\frac{\partial C}{\partial x}}_{\text{III}} - \underbrace{\frac{\partial v_g}{\partial y}\frac{\partial C}{\partial y}}_{\text{IV}} \qquad (2)$$

5  to explain the effect of deformational forces of passive tracers. When the total geostrophic tendency ($D_g/Dt$) is applied to a horizontal plane of $CO_2$ ($C$), and assuming geostrophic winds ($u_g$ and $v_g$) and no vertical motion, shear deformation (terms II and III) rotates parcels through shear vorticity, concentrating $CO_2$ gradients along lines of maximum shear (e.g. the strong shear zone south of low-pressure center in 7c),
10  while stretching deformation (terms I and IV) deforms tracers fields through stretching parallel to the shear vector such that $CO_2$ concentrates along the axis of dilation (e.g. along the cold front in 7c, d).

In the example above, deformational forces acted to enhance $CO_2$ gradients along the frontal zone and, together with the traveling cyclone-front system, helped create
15  important downstream variations. Converging wind fields are common along fronts, enhanced by frontogenesis, although the full extent of frontogenetic dynamics are not likely to be captured in the coarse resolution of the GCM used to create the transport fields of GEOS4-DAS. Nevertheless, this example demonstrates the importance of fronts, through deformation flow and advection, for transporting remotely generated
20  $CO_2$ anomalies, enhancing gradients, and causing variations that are non-local to sites thousands of kilometers away, and helps to explain the strong transient $CO_2$ variations shown in Figs. 3 and 4 and the importance of advection during frontal passage discussed in terms of the budget analysis.

Furthermore, cloudiness and precipitation are common along frontal transition
25  zones. With the above evidence that $CO_2$ anomalies concentrate along this same zone, this presents a potential problem for satellite observations of column $CO_2$ because

Full Screen / Esc

Printer-friendly Version

Interactive Discussion

frontal anomalies are likely to be hidden under clouds (Corbin and Denning, 2006). Surface observations, which measure continuously in time, are more effective for recording boundary layer variations along fronts. Continuous surface observations are therefore complementary to satellite observations, which observe much more continuously in
5  space.

In the analysis above, 60% of midlatitude frontal variations were attributed to horizontal and vertical transport through air mass exchange and deformational flow. This is not so for the tropics, where baroclinic disturbance is less prevalent, yet $CO_2$ variations during the rainy season are as large as midlatitude variations, suggesting the presence
10  of other sources for variability. Mechanisms for tropical variations are analyzed below.

### 3.4  Midlatitude vs tropical mechanisms

Sensitivity of tropical and midlatitudes PBL $CO_2$ to local and regional processes is tested with simple modeling experiments. For the control run (CONTROL), PCTM was employed as described in Sect. 2. In two sensitivity experiments, 10° square domains
15  are defined centered at grid cells in the tropics (TPJ: 3° S, 55° W) and in midlatitudes (CDL: 54° N, 105° W, SGP: 37° N, 97.5° W, and AMT: 45° N, 69° W). The domains are shown in Fig. 8. In the first experiment (NOCLOUD) sensitivity to moist convective transport was assessed by running PCTM for one year with CMF set to zero in these domains. Cloud-radiative NEE forcing still occurs offline in SiB3, but CMF transport in
20  PCTM does not. In the second experiment (NOFLUX), CMF is retained but NEE and FF surface fluxes are set to zero in the same 10° domains.

We must define and justify some terminology before proceeding. The four budget terms of interest for this analysis are: horizontal advection, vertical advection, cloud transport, and surface flux, as described in Sect. 3.2. We define non-local dynamics to
25  be regional synoptic processes acting on the 10° domains that help to cause variations at the designated sites within these domains. These terms include horizontal and vertical advection, which are controlled by synoptic meteorology and act to transport $CO_2$ anomalies laterally and vertically. Local dynamics are defined to be mesoscale

**Synoptic $CO_2$ mechanisms**

N. Parazoo et al.

⏮          ⏭

◀          ▶

Back          Close

Full Screen / Esc

Printer-friendly Version

Interactive Discussion

processes that act within the 10° domains and cause variations local to one grid cell. These include moist convection and surface flux.

Figure 9 (top row) shows monthly standard deviations of midday observed and simulated CO$_2$ for each site and run. NOFLUX causes standard deviations to decrease relative to CONTROL at each site, but by a much larger percentage in the tropics such that local variations are greatly reduced. In NOCLOUD, variations are insensitive to moist convection at AMT and CDL, mildly sensitive at SGP, and strongly sensitive at TPJ. These simulations suggest tropical variations are more sensitive to local surface flux and moist convection than in midlatitudes. Despite excluding local surface flux in one experiment and moist convection in the other, strong midlatitude variations are retained in both cases, implying that the advection terms are creating variations in the absence of local processes. The bottom row of Fig. 9, which shows monthly standard deviations of budget advection and cloud transport (as described earlier) for CONTROL, demonstrates that horizontal CO$_2$ advection contributes more to variability in midlatitudes than does moist convective transport, but that moist convection contributes more than horizontal advection in our one tropical case. Table 2 quantifies percent contributions from individual terms of the budget equation at each of these sites for an entire year. This illustrates the discrepancy between the midlatitudes and tropics in total advection (vertical+horizontal), cloud transport, and surface flux, with advection weaker and surface flux and cloud transport stronger in the tropics.

These experiments suggest different physical controls on day-to-day CO$_2$ variations in the midlatitudes and tropics. Important controls in midlatitudes are local (surface flux is 52% on average at the three North American sites) and non-local (horizontal and vertical advection combined account for 46% on average), with cloud transportmoist convection contributing only 3% on average. Tropical variations, on the other hand, appear to be more strongly sensitive to local processes in which clouds (11% of total) and surface flux (74%) dominate over advection (15%) in the annual budget. These tropical budget contributions are suggestive of a coupling of local processes where PBL CO$_2$ recharges from surface fluxes and discharges vertically through convective

transport. The simulations suggest that this may be particularly true during the wet season (~December–April), where simulated NEE is typically positive (Baker et al., 2008). We find that simulated $CO_2$ variability more than doubles in NOCLOUD and is strongly damped in NOFLUX. These simulations also suggest that regional transport in the tropics must be occurring frequently enough to prevent boundless $CO_2$ growth in NOCLOUD.

We find that variations in the tropics are just as large as those in midlatitudes but caused for different reasons. Synoptic variations in the tropics appear to be sensitive to a coupling of surface flux and moist convective transport. The importance of convective transport implies that much of the $CO_2$ anomalies created within the boundary layer are transported to the upper troposphere by moist convection and hidden from surface towers, and, with regard to inverse modeling, need to be accounted for either with proper modeling techniques and/or through upper air $CO_2$ observations.

## 4  Summary and conclusions

Continuous in-situ observations in North America, South America, and Europe suggest that strong synoptic variations occur year round, but atmospheric circulation differences cause different primary mechanisms for variations in midlatitude and tropical regions. Analysis of observed and simulated summer frontal $CO_2$ climatologies show that cold fronts are important for large scale mixing and local midlatitude synoptic variations. A frontal case study suggests that deformational flow along fronts tends to create and maintain anomalous $CO_2$ signals from the surrounding environment, and that these anomalies can then advect along with fronts as they migrate across the continent. Furthermore, these frontal anomalies are likely to be hidden under clouds due to moist convection associated with fronts. Well-calibrated, in-situ continuous continental $CO_2$ measurements are, therefore, a required complement to satellite observations.

Because of fundamental differences in atmospheric circulation in the tropics and midlatitudes, this study sought out to understand and quantify physical and biological

mechanisms in the midlatitudes and tropics responsible for strong observed synoptic $CO_2$ variations in the two regions. Boundary layer budget analysis, combined with cloud and surface flux sensitivity experiments, suggest that regional advective processes, including those associated with fronts, are major sources for synoptic $CO_2$ variability in midlatitudes, whereas strong coupling between convective transport and surface $CO_2$ flux is most important in the tropics, where baroclinically induced synoptic transport is much weaker. With more continuous $CO_2$ observations becoming available in the tropics, future work should extend the mechanistic analysis to additional tropical locations.

# References

Andres, R. J., Marland,G., Fung, I., and Matthews, E.: A 1 degrees × 1 degrees distribution of carbon dioxide emissions from fossil fuel consumption and cement manufacture, 1950–1990, Global Biogeochem. Cy., 10, 419–429, 1996.

Baker, I. T., Denning, A. S., Hanan, N., Prihodko, L., Vidale, P.-L. Davis, K., and Bakwin, P.: Simulated and observed fluxes of sensible and latent heat and $CO_2$ at the WLEF-TV Tower using SiB2.5, Global Change Biol., 9, 1262–1277, 2003.

Baker, I. T., Prihodko,L., Denning, S., Goulden, M., Miller, S., and Da Rocha, H. R.: Seasonal Drought Stress in the Amazon: Reconciling Models and Observations, J. Geophys. Res., doi:10.1029/2007JG000644, 2008, in press.

Bloom, S., da Silva, A., and Dee, D.: Documentation and Validation of the Goddard Earth Observing System (GEOS) Data Assimilation System, Version 4. Technical Report Series on Global Modeling and Data Assimilation, 2005.

Chan, D., Yuen, C. W., Higuchi, K., Shashkov, A., Liu, J., Chen, J., and Worthy, D.: On the $CO_2$ exchange between the atmosphere and the biosphere: the role of synoptic and mesoscale processes, Tellus, 56B, 194–212, 2004.

Clarke, L. C. and Renard, R. J.: Experiments in numerical objective frontal analysis, Mon. Weather Rev., 93, 547–556, 1965.

Corbin, K. D., Denning, A. S.: Using continuous data to estimate clear-sky errors in inversion of satellite $CO_2$ measurements, Geophys. Res. Lett., 33, LI2810, doi:10.1029/2006GL025910, 2006.

Dai, Y., Zeng, X., Dickinson, R. E., Baker, I., Bonan, G., Bosilovich, M., Denning, S., Dirmeyer, P., Houser, P., Niu, G., Oleson,K., Schlosser,A., and Yang, Z.-L.: The common land model, B. Am. Meteorol. Soc., 84, 1013–1023, 2003.

Davis, K. J., Bakwin, P. S., Yi, C., Berger, B. W., Zhao, C., Teclaw, R. M., and Isebrands, J. G.: The annual cycle of $CO_2$ and $H_2O$ exchange over a northern mixed forest as observed from a very tall tower, Global Change Biol., 9, 1278–1293, 2003.

Denning, A. S., Collatz, J. G., Zhang, C., Randall, D. A., Berry, J. A., et al: Simulations of terrestrial carbon metabolism and atmospheric $CO_2$ in a general circulation model. Part 1: Surface carbon fluxes, Tellus, 48B, 521–542, 1996a.

Gamnitzer, U., Karstens, U., Kromer, B., Neubert, R. E. M., Meijer, H. A. J., Schroeder, H., and Levin, I.: Carbon monoxide: A quantitative tracer for fossil fuel $CO_2$, J. Geophys. Res., 111, D22302, doi:10.1029/2005JD006966, 2006.

Geels, C., Doney, S. C., Dargaville, R., Brandt, J., and Christensen, J. H.: Investigating the sources of synoptic variability in atmospheric $CO_2$ measurements over the Northern Hemisphere continents: a regional model study, Tellus, 56B, 35–50, 2004.

Gerbig, C., Lin, J. C., Wofsy, S. C., Daube, B. C., Andrews, A. E., Stephens, B. B., Bakwin, P. S., and Grainger, C. A.: Toward constraining regional-scale fluxes of $CO_2$ with atmospheric observations over a continent: 2. Analysis of COBRA data using a receptor-oriented framework, J. Geophys. Res., 108(D24), 4757, doi:10.1029/2003JD003770, 2003.

Hack, J. J.: Parameterization of moist convection in the National Center for Atmospheric Research community climate model (CCM2), J. Geophys. Res., 99, 5551–5568, 1994.

Hanan, N. P., Berry, J. A., Verma, S. B., Walter-Shea, E. A., Suyker, A. E., Burba, G. G., and

Denning, A. Scott: Testing a model of $CO_2$, water and energy exchange in Great Plains tall-grass prairie and wheat ecosystems, Agricultural and Forest Meteorology, 131, 162–179, 2005.

Haszpra, L., Barcza, Z., Bakwin, P. S., Berger, B. W., Davis, K. J., and Weidinger, T.: Measuring system for the long-term monitoring of biosphere/atmosphere exchange of carbon dioxide, J. Geophys. Res., 106D, 3057–3070, 2001.

Holton, J. R.: An Introduction to Dynamic Meteorology, Third Edition, Elsevier, San Diego, CA, 1992.

Huffman, G. J., Adler, R. F., Morrissey, M., Bolvin, D. T., Curtis, S., Joyce, R., McGavock, B., and Susskind, J.: Global Precipitation at One Degree Daily Resolution from Multi-Satellite Observations, J. Hydrometeor, 2, 36–50, 2001.

Law, R. M., Rayner, P. J., Steele, L. P., and Enting, I. G.: Using high temporal frequency data for CO2 inversions, Global Biogeochem. Cy., 16(4), 1053, doi:10.1029/2001GB001593, 2002.

Kawa, S. R., Erickson III, D. J., Pawson,S., and Zhu, Z.: Global $CO_2$ transport simulations using meteorological data from the NASA data assimilation system, J. Geophys. Res., 109, D18312, doi:10.1029/2004JD004554, 2004.

Kiehl, J. T., Hack,J. J., Bonan, G. B., Boville, B. A., Williamson, D. L., and Rasch, P. J.: The National Center for Atmospheric Research Community Climate Model: CCM3, J. Climate, 11, 1131–1149, 1998.

Lin, J. C., Gerbig, C., Wofsy, S. C., Andrews ,A. E., Daube, B. C., Grainger, C. A., Stephens, B. B., Bakwin, P. S., and Hollinger, D. Y.: Measuring fluxes of trace gases at regional scales by Lagrangian observations: Application to the CO2 Budget and Rectification Airborne (CO-BRA) study, J. Geophys. Res., 109, D15304, doi:10.1029/2004JD004754, 2004.

Schultz, D. M.: A review of cold fronts with prefrontal troughs and wind shifts, Mon. Weather Rev., 133, 8, 2449–2472, 2005.

Sellers, P. J., Mint Z. Y., Sud, Y. C., Dalcher,A.: A simple biosphere model (SiB) for use within general circulation models, J. Atmos. Sci., 43, 505–531, 1986.

Sellers, P. J., Randall, D. A., Collatz, G. J., et al.: A revised land-surface parameterization (SiB2) for atmospheric GCMs. Part 1: Model formulation, J. Climate, 1, 676–705, 1996a.

Stohl, A., Berg, T., Burkhart, J. F., Fjæraa, A. M., Forster, C., Herber, A., Lunder, C., McMillan, W. W. , Oltmans, S., Shiobara, M. , Simpson, D., Solberg, S., Stebel, K., Ström, J., Tørseth, K., Treffeisen, R., Virkkunen, K., and Yttri, K. E.: Arctic smoke - record high air pollution levels in the European Arctic due to agricultural fires in Eastern Europe in spring 2006,

Title Page

Abstract | Introduction

Conclusions | References

Tables | Figures

◄◄ | ►►

◄ | ►

Back | Close

Full Screen / Esc

Printer-friendly Version

Interactive Discussion

Atmos. Chem. Phys., 7, 511–534, 2007,
http://www.atmos-chem-phys.net/7/511/2007/.

Takahashi, T. S., Sutherland, S. C., Sweeney, C., Poisson, A. , Metzl, N., Tilbrook, B., Bates, N., Feely, R. A., Sabine, C., Olafsson, J., and Nojiri, Y.: Global Sea-Air CO2 flux based on climatological surface ocean $pCO_2$ and seasonal biological and temperature effects, Deep-Sea Res. II, 49, 1601–1622, 2002.

Vidale, P. L. and Stockli, R.: Prognostic canopy air space solutions for land surface exchanges, Theor. Appl. Climatol., 80, 245–257, 2005.

Worthy, D. E., Higuchi, K., and Chan, D.: North American influence on atmospheric carbon dioxide data collected at Sable Island, Canada, Tellus, 55B, 105–114, 2003.

Zhang, G. J. and McFarlane, N. A.: Sensitivity of climate simulations to the parameterizations of cumulus convection in the Canadian climate center general-circulation model, Atmos. Ocean, 33, 407–446, 1995.

Title Page

Abstract | Introduction

Conclusions | References

Tables | Figures

◄ | ►|

◄ | ►

Back | Close

Full Screen / Esc

Printer-friendly Version

Interactive Discussion

**Table 1.** Description of Continuous Sites. Station ID corresponds with locations in Fig. 2.

| Station ID | Station Name | Station Description |
|---|---|---|
| LEF | Park Falls | Northern Wisconsin; surrounded by mixed forest, wetlands, agriculture, and heavy population to the SE |
| FRS | Fraserdale | South of the Hudson Bay Lowland and north of the boreal forest |
| SGP | Southern Great Plains | Great Plains of North America in a region of strong moisture gradient, characterized by agriculture |
| WKT | Moody | Great Plains of North America in a region of strong moisture gradient, characterized by cattle grazing |
| WPL | Western Peatland | Southern boreal forest of Canada |
| CDL | Candle Lake | Southern boreal forest of Canada |
| HRV | Harvard Forest | Northeastern United States; characterized by deciduous forest and heavy population to the south |
| AMT | Argle | Northeastern United States; characterized by deciduous forest and heavy population to the south |
| TPJ | Tapajos | Tapajos National Forest in the Amazon Basin |
| ALT | Alert | Northeastern tip of Ellesmere Island in Nunavut, remote from major industrial regions |
| BRW | Barrow | Alaskan coast of the Arctic Ocean, remote from major industrial regions |
| PAL | Pallas | Northern Finland in the subarctic at the northern limit of the northern boreal forest zone |
| SBI | Sable Island | Island off the coast of Nova Scotia under influenced by anthropogenic and terrestrial airflow of North America |
| MHD | Mace Head | West coast of Ireland with westerly exposure to the North Atlantic Ocean |
| ZEP | Zeppelin | Mountain ridge in the European Arcitc off the western coast of Spitsbergen (Stohl et al., 2006) |
| HEI | Heidelberg | Germany, fairly strong industrial influence to the east (Gamnitzer, 2006) |
| HUN | Hungary | Western Hungary, flat region surrounded by agriculture and patchy forest (Haszpra, 2001) |

**Table 2.** Annual mean percent contributions of individual terms from the PBL budget equation at AMT, CDL, SGP, and TPJ.

| Station ID | Horizontal | Vertical | Cloud | Surface Flux |
|---|---|---|---|---|
| AMT | 16% | 32% | 2% | 50% |
| CDL | 17% | 33% | 3% | 47% |
| SGP | 14% | 25% | 3% | 58% |
| TPJ | 4% | 11% | 11% | 74% |
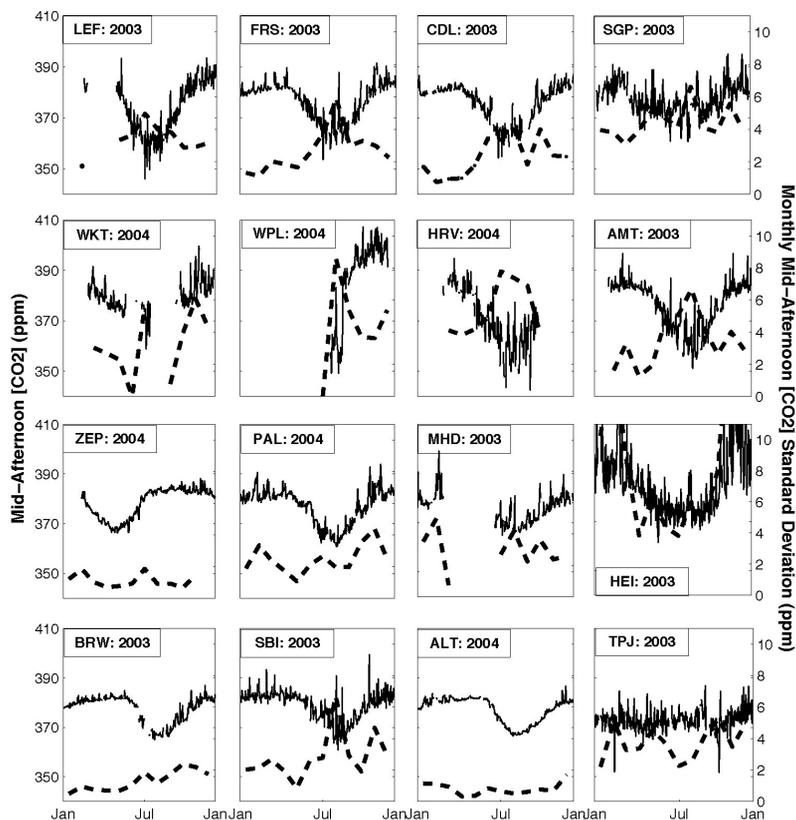
**Fig. 1.** Midday CO$_2$ (ppm) at in-situ continuous sites (solid, left y-axis) and their monthly standard deviation (dashed, right-y-axis) for 1 y.
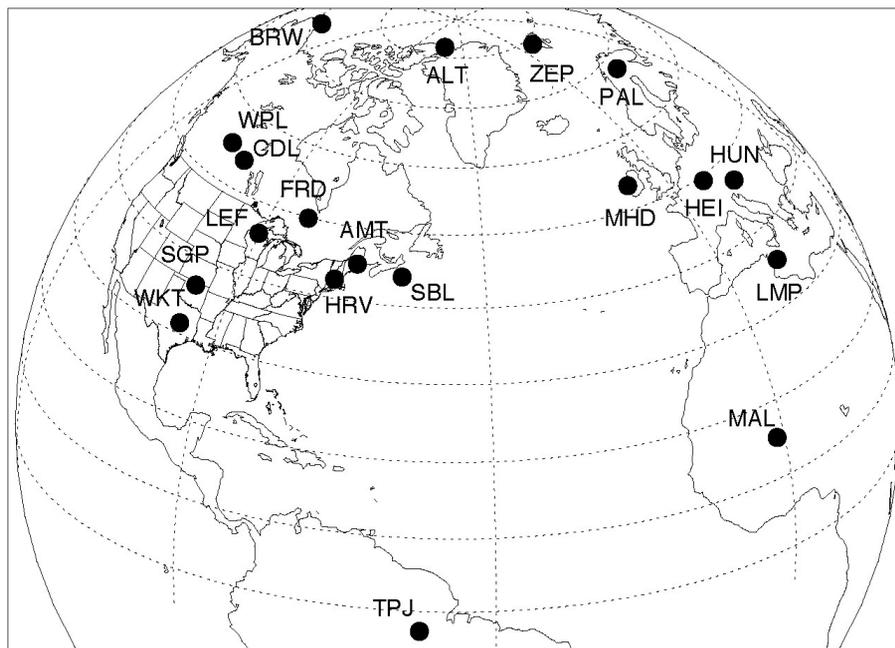
**Fig. 2.** Map of in-situ continuous sites.
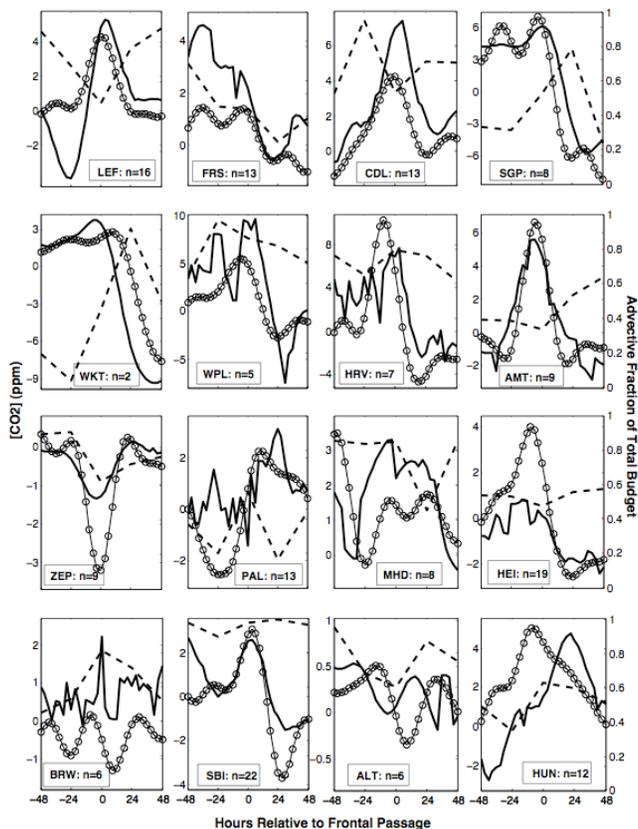
**Fig. 3.** (Left Y-Axis) Summer (JJA) climatology of observed (solid) and simulated (lowest model level in open circles) frontal CO$_2$. (Far Right Y-Axis) Total fractional contribution of daily averaged advective terms from frontal budget analysis (dashed lines). Climatologies created using method described in Sect. 3.1. The time of frontal passage is denoted by 0 on the x-axis. The station and number of events used in the averaging (*n*) is indicated within each plot.
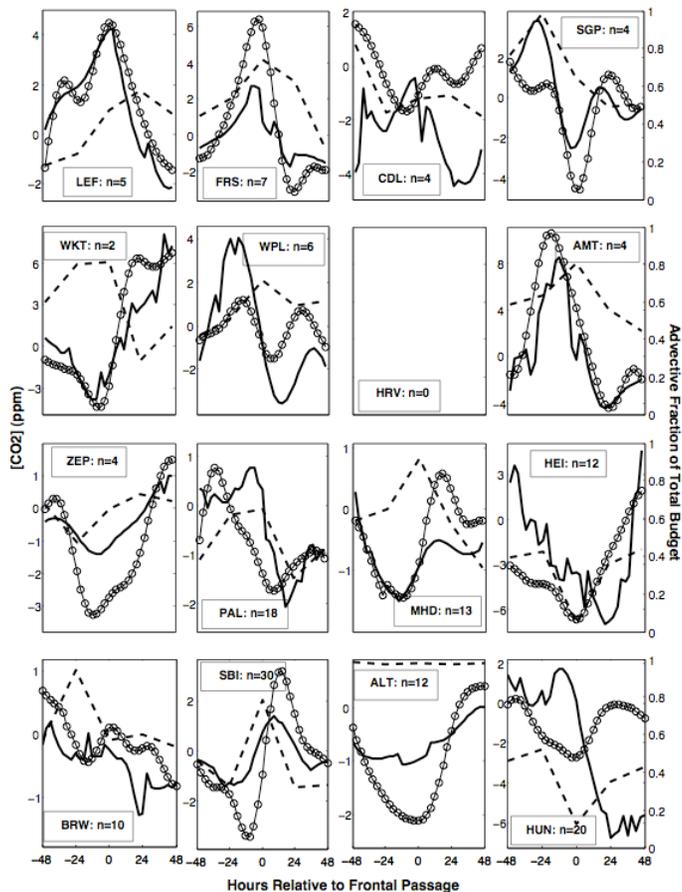
**Fig. 4.** Same as Fig. 3 except for Winter (DJF).
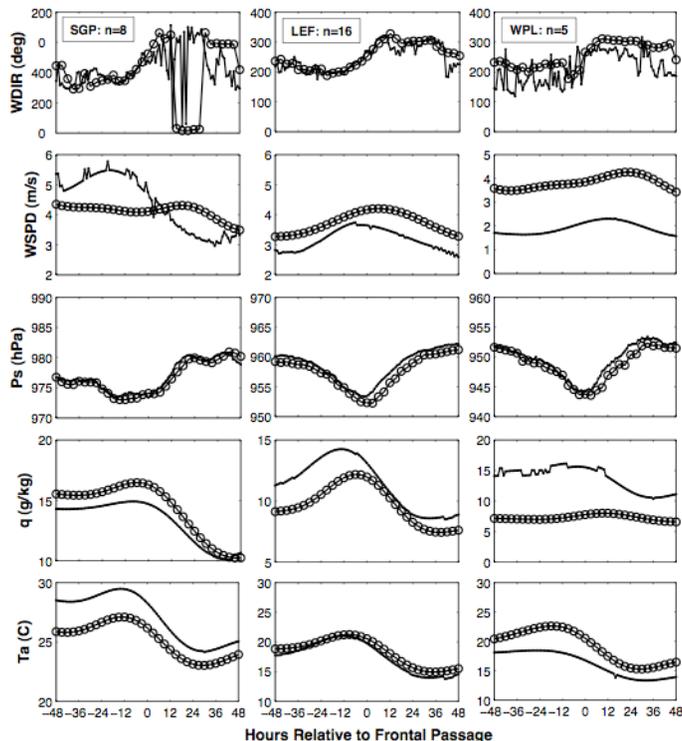
**Fig. 5.** Summer (JJA) climatology of observed (solid) and GEOS4-DAS (open circles) frontal weather fields at three North American sites. From top to bottom: Wind direction (WDIR) in degrees, wind speed (WSPD) in m/s, surface pressure ($Ps$) in hPa, specific humidity ($q$) in g/kg, and surface air temperature ($Ta$) in degrees Celsius. Observations taken at 10 m. Climatologies created using method described in Sect. 3.1. The time of frontal passage is denoted by 0 on the x-axis. The station and number of events used in the averaging ($n$) is indicated in the top row of plots, with each column representing the same station.
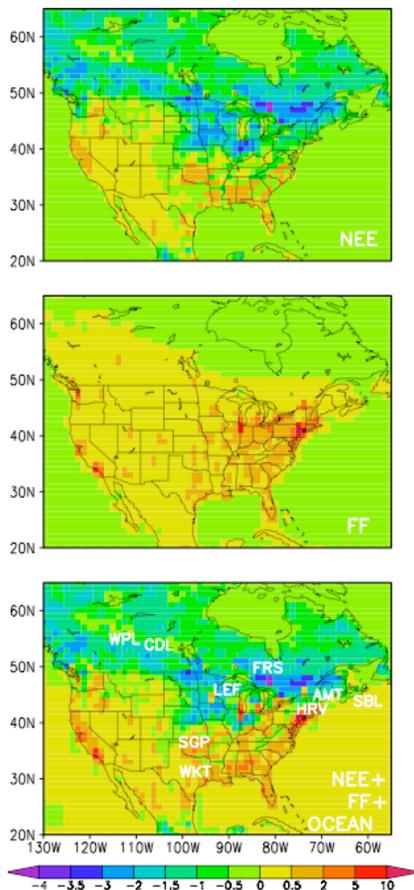
**Fig. 6.** July mean of hourly surface CO$_2$ flux of NEE (top), FF (middle), and total surface flux over land and ocean (NEE+FF+OCEAN, bottom) for North America. Each plot is on the same scale, with units of $\mu$mol/m$^2$/s, given by the color bar at the bottom. Locations of several continuous sites are plotted in the bottom plot for convenience.
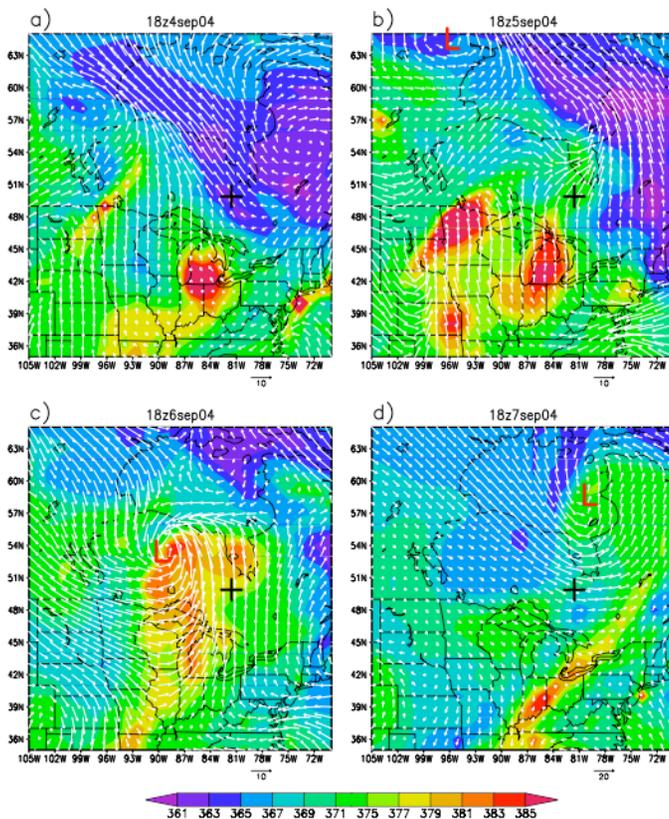
**Fig. 7.** Evolution of $CO_2$ surface anomalies (color contours) with surface winds (white vectors) as modeled over 4-day period. All times are midday (18z). The day 1 snapshot is indicated by panel **(a)**, day 2 by **(b)**, day 3 by **(c)**, and day 4 by **(d)**. The red L represents the low-pressure center of the surface cyclone migrating across the continent. The black cross indicates the location of FRS.
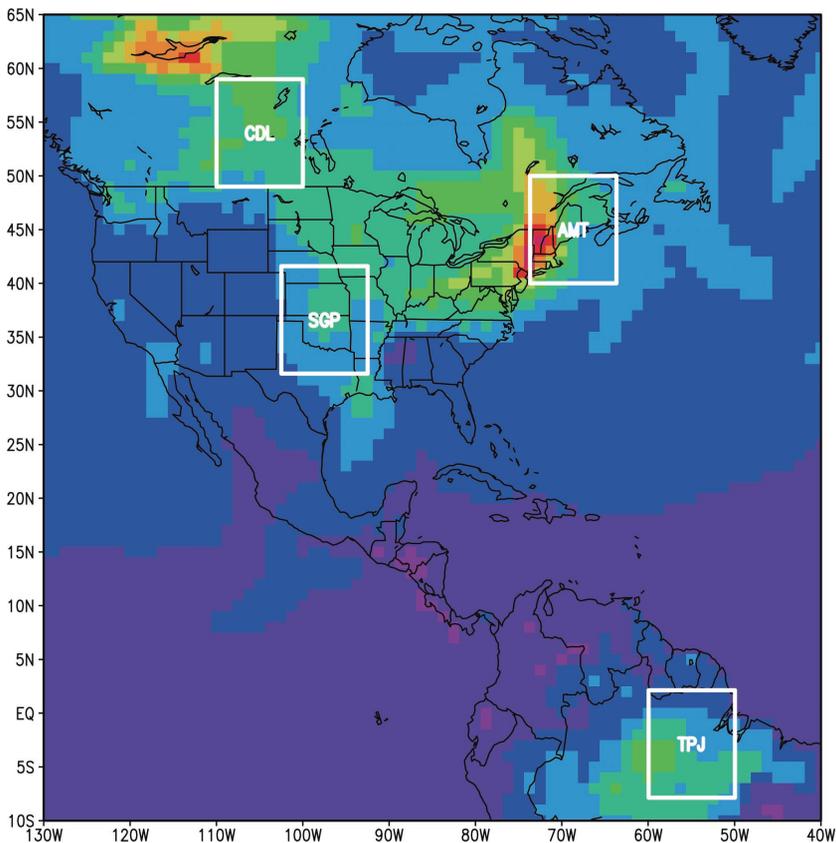
**Fig. 8.** Domains used for NOFLUX and NOCLOUD sensitivity experiments. Shading is example of CO$_2$ field at surface as simulated by PCTM.
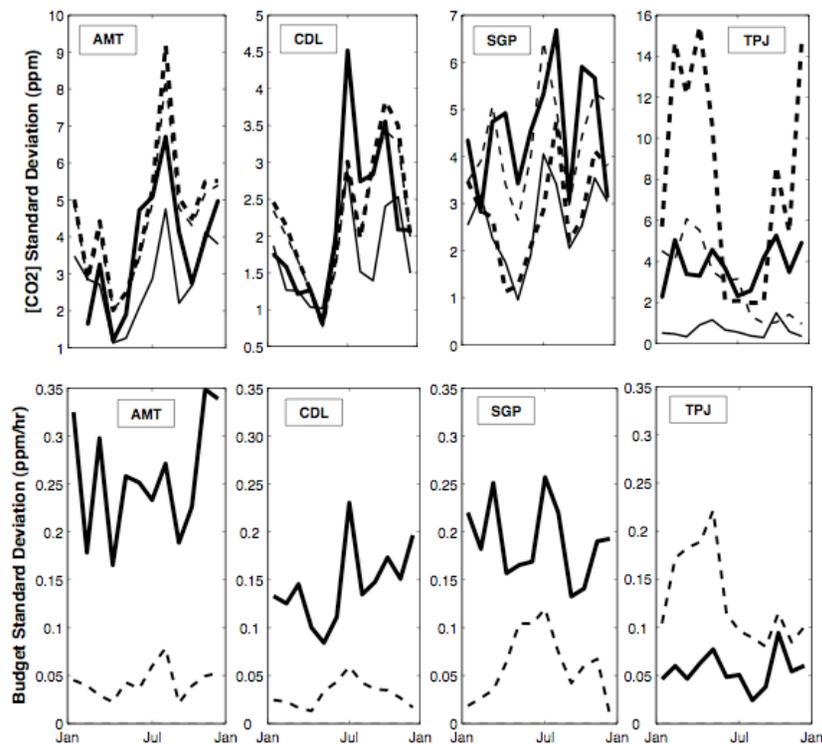
**Fig. 9.** (Top Row) Monthly standard deviation of midday CO$_2$ at grid cells containing AMT (far left), CDL (second), SGP (third) and TPJ (far right) for observations (thick solid), CONTROL (thin dashed), NOCLOUD (thick dashed), and NOFLUX (thin solid). (Bottom Row) Monthly standard deviation of horizontal advection (thick solid) and cloud transport (thin dashed) budget terms for control run.